

Spin diffusion in the low-dimensional molecular quantum Heisenberg antiferromagnet $\text{Cu}(\text{pyz})(\text{NO}_3)_2$ detected with implanted muons

F. Xiao,¹ J.S. Möller,^{2,*} T. Lancaster,¹ R.C. Williams,¹ F.L. Pratt,³
S.J. Blundell,² D. Ceresoli,⁴ A.M. Barton,⁵ and J.L. Manson⁵

¹*Durham University, Department of Physics, South Road, Durham, DH1 3LE, UK*

²*University of Oxford, Department of Physics, Clarendon Laboratory, Parks Road, Oxford, OX1 3PU, UK*

³*ISIS Pulsed Neutron and Muon Facility, STFC Rutherford Appleton Laboratory, Harwell Oxford, Didcot, OX11 0QX, UK*

⁴*Istituto di Scienze e Tecnologie Molecolari CNR, via Golgi 19, 20133 Milano, Italy*

⁵*Eastern Washington University, Department of Chemistry and Biochemistry, Cheney, Washington 99004, USA*

(Dated: December 6, 2024)

We present the results of muon-spin relaxation measurements of spin excitations in the low-dimensional quantum Heisenberg antiferromagnet $\text{Cu}(\text{pyz})(\text{NO}_3)_2$. Using density functional theory we propose the muon sites and assess the degree of perturbation the muon probe causes on the system. Our measurements of the dynamics of the system show that in the temperature range $T_N < T < J$ (between the ordering temperature T_N and the exchange energy scale J) the transport of spin excitations detected by the muon is diffusive over much of the range of applied fields. We also identify a possible cross-over in the probe response to the fluctuation spectrum at higher applied fields, to a regime where the muon detects transport with a ballistic character. This behavior is contrasted with that found for $T > J$ and that in the related two-dimensional system $\text{Cu}(\text{pyz})_2(\text{ClO}_4)_2$.

PACS numbers: 75.10.Pq, 75.50.Xx, 76.75.+i

Low-dimensional quantum magnetism continues to be of great theoretical and experimental interest as reduced dimensionality supports strong quantum fluctuations which can result in novel excitations and critical behavior¹. A notable challenge in this field is the elucidation of the mechanism for the transport of spin excitations in the one-dimensional quantum Heisenberg antiferromagnet (1DQHAF). Spin transport in this system, whose Hamiltonian is given by $\mathcal{H} = J \sum \mathbf{S}_i \cdot \mathbf{S}_{i+1}$, has been extensively studied²⁻¹⁴ but the nature of transport remains controversial, with some theoretical and numerical studies^{3,6,9} suggesting that the transport is necessarily ballistic; while others^{7,12} show it to be diffusive. More recent work has shown that when subjected to a periodic lattice potential, diffusion can co-exist with ballistic transport^{10,13}. Using implanted muons we have probed a molecular magnet which closely approximates the 1DQHAF in the temperature regime $T_N < T < J$, where we access the excitations that result from this low-dimensional behavior¹. Here we show that the excitations detected by the muon are diffusive for a large range of applied magnetic fields. We contrast this behavior with the excitations probed for $T > J$ and that of a two-dimensional (2D) molecular magnet.

Many coordination polymer molecular magnets have been shown to closely realize models of low-dimensional magnetism, with the advantage that their typical energy scales are experimentally accessible, in contrast to many oxide materials. Coordination polymers comprise regular arrays of transition metal ions (e.g. $S = 1/2$ Cu^{2+}) linked with molecular ligands such as pyrazine ($\text{pyz} = \text{C}_4\text{H}_4\text{N}_2$). The low-dimensional structural motifs that may be realised in these materials have been shown to promote low-dimensional magnetic behavior. $\text{Cu}(\text{pyz})(\text{NO}_3)_2$ consists of well-isolated Cu-pyz-Cu chains and has been shown

to be a highly successful realization of the 1DQHAF, with a principal exchange constant of $J = 10.3(1) \text{ K}^{15} [= 7.2(1) \times 10^3 \text{ mT}^{16}]$. Although theoretically we expect an ideal 1DQHAF to remain disordered at all temperatures (its ground state is a Tomonaga-Luttinger liquid with a gapless spectrum of excitations with linear dispersion), a real system is expected to undergo long-range magnetic ordering due to the weak coupling between spin chains. $\text{Cu}(\text{pyz})(\text{NO}_3)_2$ orders at $T_N = 0.107(1) \text{ K}$, leading to an estimate of the interchain-intrachain coupling ratio of¹⁷ $J_{\perp}/J_{\parallel} \approx 4.4 \times 10^{-3}$. Inelastic neutron scattering (INS) measurements at 0.25 K reveal the expected spinon excitation spectrum^{15,18} while NMR experiments demonstrate that a shift of the maximum of field-dependent relaxation rate T_1^{-1} in the system is caused by spin-spin interactions¹⁹. We also present results of measurements on the 2D material $\text{Cu}(\text{pyz})_2(\text{ClO}_4)_2$ which belongs to a family of 2DQHAFs^{20,21} in which Cu ions sit at the corners of a square lattice and are linked by pyrazine molecules. Here the interaction strength J is found to be $17.5(3) \text{ K}^{20}$ and the system orders at $4.2(1) \text{ K}^{22}$, resulting in an exchange anisotropy of $J_{\perp}/J \approx 5 \times 10^{-4}$.

In a muon-spin relaxation ($\mu^+\text{SR}$) experiment²³ spin-polarized muons are implanted into the sample. The quantity of interest is the asymmetry $A(t)$, which is proportional to the average spin polarization of the muon ensemble. Muons have been shown to be sensitive probes of low-dimensional magnets, not only revealing the ordering temperatures in $\text{Cu}(\text{pyz})_2(\text{NO}_3)_2$ ¹⁷, but also being sensitive to the nature of the spin excitations in the MHz frequency range, allowing the identification of diffusive and ballistic behavior. For example, the study of the molecular radical 1DQHAF DEOCC-TCNQF₄²⁴ identified diffusive transport while in the inorganic 1DQHAF

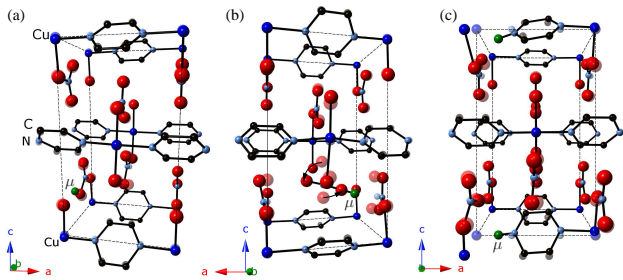


FIG. 1. The diamagnetic muon sites in $\text{Cu}(\text{pyz})(\text{NO}_3)_2$. Translucent spheres represent the ionic positions in the unit cell without the muon. (a) The nitrate site (bonding oxygen moved by 0.4 \AA , other ions move by $\leq 0.2 \text{ \AA}$). (b) The nitrate site with the nearly 90° rotation of the nitrate group around the b -axis (oxygen ions moved by $1.5, 1.2, 0.3 \text{ \AA}$). (c) The nitrogen site (Cu ion moved by 1.4 \AA).

$\text{Rb}_4\text{Cu}(\text{MoO}_4)_3$ ballistic transport was shown to dominate²⁵. To complement our μ^+ SR results described below along with those of a previous zero-field (ZF) muon experiment¹⁷ that revealed long-range magnetic order below $T_N = 0.107(1) \text{ K}$, we have performed density-functional theory (DFT) calculations to investigate the stopping sites of the muon in $\text{Cu}(\text{pyz})(\text{NO}_3)_2$ and the extent of the perturbation the muon exhibits locally²⁶. Prior to the ZF μ^+ SR measurement, magnetic ordering had not been detected in heat capacity measurements down to 0.070 K ²⁷. This may be explained by noting that in low-dimensional systems the onset of correlations above the magnetic ordering temperature reduces the amount of entropy ejected upon ordering and thereby reduces the specific heat response to magnetic ordering²⁸. However, DFT also allows us to investigate whether the muon itself could give a spurious indication of order owing to the local electronic distortion that it creates.

DFT calculations were performed for both positively charged and neutral supercells; the former corresponds to the scenario where the muon (modelled by a norm-conserving hydrogen pseudopotential) does not attract an electron through some thermal or epithermal process during the stopping process. Note however that in the calculations the muon loses the extra electron in the $\text{N}(\text{pyz})$ and NO_3^- sites in the neutral supercell described below. The structural relaxations reveal two classes of diamagnetic muon site, (with negligible contact hyperfine coupling). In the first site [Fig. 1(a)] the muon forms a hydroxyl-type bond with any one of the three inequivalent oxygen ions in the nitrate group (denoted as NO_3^- site). Here the muon is approximately coplanar with the nitrogen and oxygen ions (within 3°). This site exists in both neutral and charged supercells. In the neutral supercell an additional site is predicted where the presence of the muon leads to the rotation of the entire bonding nitrate group by nearly 90 degrees around the b -axis [Fig. 1(b)]. The muon remains coplanar with the other atoms in the nitrate group (within 7°). Other than this rotation, the crystallographic distortions in this site are

$\leq 0.6 \text{ \AA}$ for atoms not in the bonding nitrate group. In the second diamagnetic site [denoted $\text{N}(\text{pyz})$] the muon bonds to one of the two equivalent nitrogen atoms in either pyrazine ring [Fig. 1(c)]. As this nitrogen atom is very close to the Cu ion, the crystallographic distortion of the Cu ion *is* significant ($> 1 \text{ \AA}$). This site exists in both the charged and the neutral supercell. In addition to the diamagnetic sites a high-energy radical site was found in both neutral and charged supercells, where the muon bonds to one of the four equivalent carbon atoms in the pyrazine ring. In the neutral cell, interstitial muonium (Mu) was also predicted, though at an energy considerably above the diamagnetic states described above. Finally, it is conceivable that the muon may substitute for any of the four equivalent hydrogen atoms in either pyrazine ring though the energy of such a state depends on the final state of the substituted proton²⁶. As shown in the Supplemental Information²⁶, the calculated sites are consistent with the experimentally measured muon precession frequencies.

Next we consider the perturbation of the local magnetic structure caused by the muon. For the neutral supercell, the muon in the NO_3^- or $\text{N}(\text{pyz})$ sites donates its electron to the nearest-neighbor Cu ion, turning the magnetic Cu^{2+} ion into diamagnetic Cu^+ . This acts to interrupt the Cu-pyz-Cu exchange pathway and reduces the dipolar coupling of the muon significantly for most magnetic structures. Furthermore the Cu^{1+} environment distorts away from square-planar towards a linear N-Cu-N “dumbbell” arrangement [note the displacement of the oxygen ions in Fig. 1(b)]. This is consistent with the observation that $\text{Cu}^{1+} 3d^{10}$ ions prefer linear coordination in order to reduce the orbital overlap with the ligands. In the $\text{N}(\text{pyz})$ site, there is therefore a combined effect of (i) switching off the magnetic moment through this mechanism and (ii) the structural distortion of the Cu ion, while in the charged supercell only the structural distortion is present, leading to increased magnetic overlap between adjacent Cu-pyz-Cu chains via a nitrate group²⁶. Note that for the $\text{N}(\text{pyz})$ site the distortion of the Cu environment is more significant and, for the neutral cell, cannot be explained with a reduced orbital overlap with its ligands alone. While all of these are significant local perturbations that affect the measured dipolar coupling, it is unlikely that any of these would be capable of condensing long-range magnetic order. The states formed by a single spin $S = 1/2$ impurity coupling to a spin-chain have been studied in detail theoretically, both numerically and using conformal field theory²⁹. The result is a prediction that the coupling of a muon impurity to a $S = 1/2$ Cu^{2+} spin in a 1DQHAF would result in a screened spin with effective $S = 0$, whose influence on the local susceptibility is healed with increasing distance from the defect. In a μ^+ SR experiment, muons are implanted in the ultradilute limit, so that the chance of muons catalysing any sort of collective state or influencing each other is effectively zero. Previously¹⁷, oscillations at two dominant frequencies were observed in the magnetically or-

dered state, along with evidence for at least one other class of muon site which did not give rise to a resolvable precession signal. It is therefore possible that the two frequencies result from the less-perturbative nitrate site (i.e. the charged cell), where neither magnetic- nor crystal structure are significantly perturbed and where the muon is unlikely to have a strong coupling to a single Cu^{2+} and enter into the singlet state. The remainder of the signal (i.e. the non-oscillatory contribution) might then result from the N(pyz) sites and the more perturbative nitrate site (neutral cell), whose interaction with the spin chain would be more complicated.

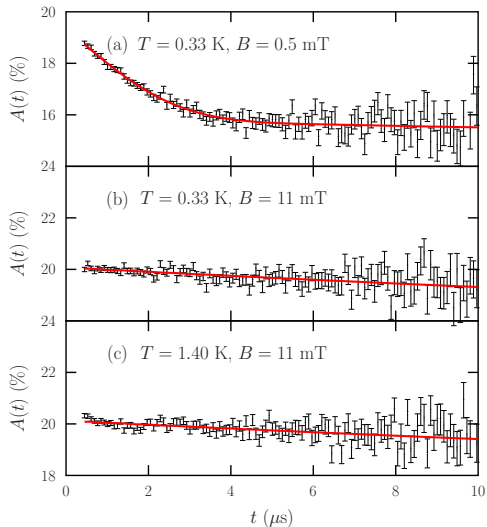


FIG. 2. (Color online.) Example $A(t)$ spectra for $\text{Cu}(\text{pyz})(\text{NO}_3)_2$ at (a) $T = 0.33$ K and $B = 0.5$ mT (b) $T = 0.33$ K and $B = 11$ mT (c) $T = 1.40$ K and $B = 11$ mT. Solid lines represent the fits described in the text.

We now turn to the results of our longitudinal field (LF) μ^+ SR measurements, where an applied external magnetic field is directed parallel to the initial muon spin directions and decouples the contribution from static magnetic fields at the muon site. This allows us to probe the dynamics of the system, as time-varying magnetic fields at the muon site are able to flip muon spins. LF μ^+ SR measurements were made on powder samples of $\text{Cu}(\text{pyz})(\text{NO}_3)_2$ and $\text{Cu}(\text{pyz})_2(\text{ClO}_4)_2$ using the EMU spectrometer at the ISIS facility, UK at several temperatures [$T = 0.33$ K, 1.4 K and 15 K for $\text{Cu}(\text{pyz})(\text{NO}_3)_2$ and $T = 4.6$ K for $\text{Cu}(\text{pyz})_2(\text{ClO}_4)_2$]. Samples were packed in Ag foil envelopes (foil thickness $12.5\mu\text{m}$) and mounted on an Ag plate using vacuum grease before being attached to either the cold finger of a sorption cryostat (for $0.3 < T < 1.5$ K) or loaded into a ^4He cryostat for $T > 1.5$ K measurements.

Example LF μ^+ SR spectra measured for $\text{Cu}(\text{pyz})(\text{NO}_3)_2$ at temperatures $T > T_N$ are shown in Fig. 2. In applied magnetic fields of $B \lesssim 0.5$ mT, the asymmetry shows Kubo-Toyabe relaxation³⁰ due to the disordered magnetic fields from the nuclei surrounding

the muon sites. The contribution from the nuclei, however, is suppressed when the applied field increases and the asymmetry shows only a slow exponential relaxation. The asymmetry $A(t)$ spectra were fitted to the function $A(t) = A_{\text{rel}}G_z^{\text{KT}}(\Delta, B)e^{-\lambda t} + A_{\text{bg}}$, which includes the contribution from both the nuclei and electronic moments. Here A_{rel} is the amplitude of the relaxing component, $G_z^{\text{KT}}(\Delta, B)$ is the Kubo-Toyabe relaxation function, λ is the relaxation rate reflecting slow dynamics of the electronic spins and A_{bg} accounts for the constant background contribution. For both $\text{Cu}(\text{pyz})(\text{NO}_3)_2$ and $\text{Cu}(\text{pyz})_2(\text{ClO}_4)_2$ the field width Δ was fixed at around 0.3 MHz. The values of λ from the fitting routine are plotted against applied magnetic field in Fig. 3. In all cases described below, the relaxation rates show a similar (approximately power-law-like) decrease at the low fields ($B \lesssim 6$ mT) before developing distinct behaviors at higher fields ($B \gtrsim 6$ mT). It is most likely that the low field behavior, which does not significantly vary with temperature, is dominated by nuclear magnetism and that the nuclear contribution is effectively quenched above 6 mT. Therefore the behavior of λ in the low field regime ($B \lesssim 6$ mT) is excluded from any further discussion.

The B -dependence of the relaxation rate can be used to determine the nature of transport of spin excitation (i.e. whether ballistic or diffusive) as the spin auto-correlation functions have different spectral densities in the two cases. For diffusive transport, the spectral density $f(\omega)$ has the form $f(\omega) \sim \omega^{-1/2}$, which leads to a $\lambda \propto B^{-1/2}$ power-law relation. In contrast, for ballistic transport, $f(\omega)$ follows a logarithmic relation $f(\omega) \sim \ln(J/\omega)$, or $\lambda \propto \ln(J/B)$. We note that for the calculated muon sites discussed above, a possible (avoided) level crossing resonance occurs at approximately 140 mT due to a pure muon spin flip ($\Delta M = 1$)²⁶. We expect that this resonance possesses only a small signal amplitude and is relatively narrow (on the order of 10 mT) and hence do not expect it to affect the conclusions drawn below, which are based on the scaling behavior of λ over wide ranges in field.

Three models were used to fit the relaxation rate λ (summarised in Table I). In the temperature regime $T_N < T < J$, where we expect the spin transport models to apply, we first attempt to fit all data for $B \gtrsim 6$ mT to the ballistic transport function $\lambda = c \ln(J/B)$ (Model II in Table I). This results in unacceptably small values of the intrachain exchange constant J , where we obtain $J = 1.4(4) \times 10^3$ mT at $T = 0.33$ K and $1.1(3) \times 10^3$ mT at 1.40 K. These compare poorly with the value $J = 7.2 \times 10^3$ mT, inferred from magnetic susceptibility measurements and suggests that the ballistic model does not apply over this range. We also fit all data for $B \gtrsim 6$ mT to a power law function $\lambda = aB^{-n}$ (Model I) with a constant a , but the fit quality is poor due to the fact that λ flattens out above 100 mT at both $T = 0.33$ K and $T = 1.40$ K. The fitted exponent n [0.35(3) for $T = 0.33$ K and 0.36(3) for $T = 1.40$ K] is also smaller

	diffusive Model I: $\lambda = aB^{-n}$ $6 \text{ mT} \lesssim B \lesssim 100 \text{ mT}$	ballistic Model II: $\lambda = c \ln(J/B)$ $6 \text{ mT} \lesssim B \lesssim 450 \text{ mT}$	ballistic Model III: $\lambda = c \ln(J/B)$ $50 \text{ mT} \lesssim B \lesssim 450 \text{ mT}$
$T = 0.33 \text{ K}$	$a = 0.16(3), n = 0.42(4)$	$c = 0.004(1), J = 1.4(4) \times 10^3 \text{ mT}$	$c = 0.0025(2)$
$T = 1.40 \text{ K}$	$a = 0.17(4), n = 0.42(5)$	$c = 0.005(1), J = 1.1(3) \times 10^3 \text{ mT}$	$c = 0.0026(2)$
$T = 15 \text{ K}$	$a = 0.13(2), n = 0.21(3)$	$c = 0.009(1), J = 1.8(5) \times 10^3 \text{ mT}$	$c = 0.0063(3)$

TABLE I. Fitted coefficients for $\text{Cu}(\text{pyz})(\text{NO}_3)_2$. The exchange J was fixed at the known value of $7.2 \times 10^3 \text{ mT}$ in Model III.

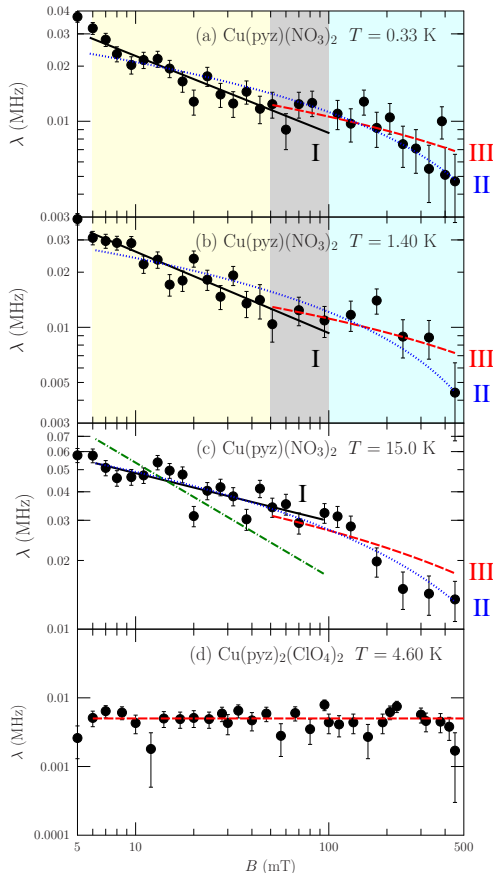


FIG. 3. (Color online.) (a-c) Relaxation rates λ for $\text{Cu}(\text{pyz})(\text{NO}_3)_2$. Solid lines: power law fit; dotted lines: global fit to ballistic behavior; dashed lines: fit to ballistic behavior between 50 mT and 500 mT with J fixed at $7.2 \times 10^3 \text{ mT}$. (c) dot dash line: an example power-law function with fixed $n = 0.5$. (d) Relaxation rates λ for $\text{Cu}(\text{pyz})_2(\text{ClO}_4)_2$; dashed line: linear fit function.

than expected for a 1DQHAF ($n = 0.5$).

In contrast, we find that the data can be best described with the power law expression for B in the range $6 \text{ mT} \lesssim B \lesssim 100 \text{ mT}$ [solid lines in Fig. 3(a), (b)]. Fitting this model to the measured data gives $n = 0.42(4)$ at $T = 0.33 \text{ K}$ and $n = 0.42(5)$ at 1.40 K , very close to the theoretical value of $n = 0.5$. From this we infer our main result: that the spin transport detected by the muon is

diffusive in this magnetic field range.

However, λ flattens out above around 100 mT and the data is no longer well described by Model I. Intriguingly, we find that for $B \gtrsim 50 \text{ mT}$, where the power law fit fails, the data can be fitted to the predictions of the ballistic model reasonably well in the limit of high fields, with J fixed at the experimentally determined value of $7.2 \times 10^3 \text{ mT}$ (Model III). This raises the possibility that the muon probe response crosses over from detecting diffusive behavior at low fields (i.e. at low frequency) to ballistic behavior (on a shorter time scale) above $B \approx 50 \text{ mT}$. This is expected in that diffusion seen at low frequency ω should, at short times (or higher frequency), start with ballistic steps. In the present case it is possible that we are able to detect both of these parts of the fluctuation spectrum by tuning the frequency response window the the muon probe with applied magnetic field. However, there is reason to be cautious here owing to the significant experimental uncertainty arising from the sensitivity of the results to detector dead times and the resolution limit of the spectrometer for the small relaxation rates measured for fields $B \gtrsim 200 \text{ mT}$.

We may compare these results with those found outside the region of applicability of the spin transport models. In the high temperature regime $T > J$ the failure of both models is expected since the muons are responding not only to the spin excitation but also to the quasi-independent spin flips introduced by thermal fluctuations. As expected, fits of our measurements made at $T = 15 \text{ K}$ [Fig. 3(a) and Table I] show that neither the diffusive model nor the ballistic models return physically realistic parameters.

To contrast the behavior of the 1D chain, we also made measurements of the 2D material $\text{Cu}(\text{pyz})_2(\text{ClO}_4)_2$ in the region $T_N < T < J$. Similarly to the 1D chain, the asymmetry spectra of the 2D material show Kubo-Toyabe relaxation at low magnetic field which is suppressed at high fields. A difference observed in the asymmetry spectra between $\text{Cu}(\text{pyz})(\text{NO}_3)_2$ and $\text{Cu}(\text{pyz})_2(\text{ClO}_4)_2$ is that in addition to the slow relaxation, a fast exponential decay ($\Lambda \approx 2 \text{ MHz}$) persists in the asymmetry spectra up to the highest field. The total asymmetry signal was fitted to a sum of two exponential decaying components with a background contribution: $A(t) = A_s G_z^{\text{KT}}(\Delta, B) e^{-\lambda t} + A_f e^{-\Lambda t} + A_{\text{bg}}$, where A_s and A_f correspond to the amplitude of the Kubo-Toyabe

and the fast relaxing component, respectively. Here λ is the relaxation rate for the slow-relaxing component, Λ is fixed at 1.65 MHz for the fast relaxing component and A_{bg} accounts for the background contribution. From Fig 3(d), it can be seen that the relaxation rate λ shows little field dependence, remaining constant within the experimental uncertainty. In fact, it is probable that the spectrometer is close to its time resolution limit below 6 kHz.

In conclusion, we find that for 1DQHAF $\text{Cu}(\text{pyz})(\text{NO}_3)_2$ when $T_N < T < J$, the diffusive model provides a better description of the data than the ballistic model in the field range $6 \text{ mT} \lesssim B \lesssim 100 \text{ mT}$. The values of the exponent extracted from the fit to Model I [$n = 0.42(4)$ and $n = 0.42(5)$] match the theoretical prediction of $n = 0.5$ for spin diffusion model closely and there is little variation in the parameter a . We may also compare our results with that found in DEOCC-TCNQF₄, where diffusive transport was also reported. We see that our measurements are in better

agreement with theory ($n \approx 0.42$ for $\text{Cu}(\text{pyz})(\text{NO}_3)_2$, as opposed to $n \approx 0.35$ reported for DEOCC-TCNQF₄ in Ref 24) even though the latter is predicted to be a better isolated 1DQHAF on the basis of its lack of magnetic ordering down to 20 mK. In DEOCC-TCNQF₄ the diffusive behavior shows a low-field cut-off, from which the interchain-intrachain ratio J_{\perp}/J_{\parallel} can be estimated. This cut-off should scale with J_{\perp} , and should therefore occur in $\text{Cu}(\text{pyz})(\text{NO}_3)_2$ at $B \approx 2 \text{ mT}$. However, no sharp change in behavior is observed at this low field. Also contrasting with DEOCC-TCNQF₄, $\text{Cu}(\text{pyz})(\text{NO}_3)_2$ shows a crossover in the $50 \text{ mT} \lesssim B \lesssim 100 \text{ mT}$ region with the power law not describing the data well above these fields.

We are grateful to the STFC ISIS Facility for the provision of muon beamtime, the E-Infrastructure South Initiative for CPU time and EPSRC (UK) for financial support. We thank Daniel Khomskii for useful discussions. The work at EWU was supported by the U.S. National Science Foundation under grant no. DMR-1306158.

-
- * Present address: Neutron Scattering and Magnetism, Laboratory for Solid State Physics, ETH Zürich, CH-8093 Zürich, Switzerland
- ¹ S. Sachdev, *Quantum Phase Transitions*, 2nd ed. (Cambridge University Press, 2011).
 - ² S. Sachdev, *Phys. Rev. B* **50**, 13006 (1994).
 - ³ H. Castella, X. Zotos, and P. Prelovšek, *Phys. Rev. Lett.* **74**, 972 (1995).
 - ⁴ M. Takigawa, N. Motoyama, H. Eisaki, and S. Uchida, *Phys. Rev. Lett.* **76**, 4612 (1996).
 - ⁵ M. Takigawa, O. A. Starykh, A. W. Sandvik, and R. R. P. Singh, *Phys. Rev. B* **56**, 13681 (1997).
 - ⁶ B. N. Narozhny, A. J. Millis, and N. Andrei, *Phys. Rev. B* **58**, R2921 (1998).
 - ⁷ X. Zotos, *Phys. Rev. Lett.* **82**, 1764 (1999).
 - ⁸ F. Heidrich-Meisner, A. Honecker, D. C. Cabra, and W. Brenig, *Phys. Rev. B* **68**, 134436 (2003).
 - ⁹ J. Benz, T. Fukui, A. Klümper, and C. Scheeren, *Journal of the Physical Society of Japan* **74S**, 181 (2005).
 - ¹⁰ J. Sirker, R. G. Pereira, and I. Affleck, *Phys. Rev. Lett.* **103**, 216602 (2009).
 - ¹¹ S. Langer, F. Heidrich-Meisner, J. Gemmer, I. P. McCulloch, and U. Schollwöck, *Phys. Rev. B* **79**, 214409 (2009).
 - ¹² S. Grossjohann and W. Brenig, *Phys. Rev. B* **81**, 012404 (2010).
 - ¹³ J. Sirker, R. G. Pereira, and I. Affleck, *Phys. Rev. B* **83**, 035115 (2011).
 - ¹⁴ R. Steinigeweg, *EPL (Europhysics Letters)* **97**, 67001 (2012).
 - ¹⁵ P. R. Hammar, M. B. Stone, D. H. Reich, C. Broholm, P. J. Gibson, M. M. Turnbull, C. P. Landee, and M. Oshikawa, *Phys. Rev. B* **59**, 1008 (1999).
 - ¹⁶ The equation $g\mu_B J[\text{T}] = k_B J[\text{K}]$ was used to calculate the equivalent value of J in magnetic field units. The average g -value (2.13) was taken from Ref 15.
 - ¹⁷ T. Lancaster, S. J. Blundell, M. L. Brooks, P. J. Baker, F. L. Pratt, J. L. Manson, C. P. Landee, and C. Baines, *Phys. Rev. B* **73**, 020410 (2006).
 - ¹⁸ M. B. Stone, D. H. Reich, C. Broholm, K. Lefmann, C. Rischel, C. P. Landee, and M. M. Turnbull, *Phys. Rev. Lett.* **91**, 037205 (2003).
 - ¹⁹ H. Kühne, A. A. Zvyagin, M. Günther, A. P. Reyes, P. L. Kuhns, M. M. Turnbull, C. P. Landee, and H.-H. Klauss, *Phys. Rev. B* **83**, 100407 (2011).
 - ²⁰ F. M. Woodward, P. J. Gibson, G. B. Jameson, C. P. Landee, M. M. Turnbull, and R. D. Willett, *Inorganic Chemistry* **46**, 4256 (2007), pMID: 17432847.
 - ²¹ F. Xiao, F. M. Woodward, C. P. Landee, M. M. Turnbull, C. Mielke, N. Harrison, T. Lancaster, S. J. Blundell, P. J. Baker, P. Babkevich, and F. L. Pratt, *Phys. Rev. B* **79**, 134412 (2009).
 - ²² T. Lancaster, S. J. Blundell, M. L. Brooks, P. J. Baker, F. L. Pratt, J. L. Manson, M. M. Conner, F. Xiao, C. P. Landee, F. A. Chaves, S. Soriano, M. A. Novak, T. P. Papageorgiou, A. D. Bianchi, T. Herrmannsdörfer, J. Wosnitzer, and J. A. Schlueter, *Phys. Rev. B* **75**, 094421 (2007).
 - ²³ S. J. Blundell, *Contemporary Physics* **40**, 175 (1999).
 - ²⁴ F. L. Pratt, S. J. Blundell, T. Lancaster, C. Baines, and S. Takagi, *Phys. Rev. Lett.* **96**, 247203 (2006).
 - ²⁵ T. Lancaster, P. J. Baker, F. L. Pratt, S. J. Blundell, W. Hayes, and D. Prabhakaran, *Phys. Rev. B* **85**, 184404 (2012).
 - ²⁶ More details of the DFT theory and calculation are given in the Supplemental Information.
 - ²⁷ G. Mennenga, L. de Jongh, W. Huiskamp, and J. Reedijk, *Journal of Magnetism and Magnetic Materials* **44**, 89 (1984).
 - ²⁸ J. Jornet-Somoza, M. Deumal, M. A. Robb, C. P. Landee, M. M. Turnbull, R. Feyerherm, and J. J. Novoa, *Inorganic Chemistry* **49**, 1750 (2010).
 - ²⁹ S. Eggert and I. Affleck, *Phys. Rev. B* **46**, 10866 (1992).
 - ³⁰ R. S. Hayano, Y. J. Uemura, J. Imazato, N. Nishida, T. Yamazaki, and R. Kubo, *Phys. Rev. B* **20**, 850 (1979).

Supplemental information

Spin diffusion in the low-dimensional molecular quantum Heisenberg antiferromagnet $\text{Cu}(\text{pyz})_2(\text{NO}_3)_2$ detected with implanted muons

F. Xiao,¹ J.S. Möller,^{2,*} T. Lancaster,¹ R.C. Williams,¹ F.L. Pratt,³
S.J. Blundell,² D. Ceresoli,⁴ A.M. Barton,⁵ and J.L. Manson⁵

¹*Durham University, Department of Physics, South Road, Durham, DH1 3LE, UK*

²*University of Oxford, Department of Physics, Clarendon Laboratory, Parks Road, Oxford, OX1 3PU, UK*

³*ISIS Pulsed Neutron and Muon Facility, STFC Rutherford Appleton Laboratory, Harwell Oxford, Didcot, OX11 0QX, UK*

⁴*Istituto di Scienze e Tecnologie Molecolari CNR, via Golgi 19, 20133 Milano, Italy*

⁵*Eastern Washington University, Department of Chemistry and Biochemistry, Cheney, Washington 99004, USA*

(Dated: December 6, 2024)

I. COMPUTATIONAL DETAILS

A. Density-functional theory

The density-functional theory (DFT) calculations were performed with the QUANTUM ESPRESSO package¹ within the generalized-gradient approximation² (GGA) using norm-conserving and ultra-soft³ pseudopotentials. The muon was modelled by a norm-conserving hydrogen pseudopotential. The wavefunction and charge-density cutoffs were 80 and 320 Rydberg, respectively. Brillouin-zone integration was performed at the Γ point. The results reported here were obtained in calculations for a supercell of $2 \times 2 \times 1$ conventional unit cells (plus the muon). Both neutral and positively charged (+1) supercells were studied. The latter corresponds to the scenario where the muon does not attract an electron through some thermal or epithermal process during the stopping process. It is in principle possible to compare the formation energy of both of these charge states. However the band gap is underestimated by DFT and its accurate calculation would require expensive many-body techniques like the GW method.

The muon was placed in several randomly chosen sites (all with a multiplicity of 8) which were a maximum of 1.5 Å from the nearest neighbor starting site (or its crystallographic equivalent). All atoms were then allowed to relax. The structural relaxations were based on the structures measured at 2 K⁴ and used the experimental unit cell parameters. All relaxations were done in a collinear spin-polarized calculation with magnetic propagation vector (1/2 0 0) (for the conventional unit cell).

Allowing the ionic positions in the supercell without the muon to relax from the experimentally known positions yields negligible relaxation (< 0.1 Å). For the relaxed supercell, the Löwdin analysis yields a Cu^{2+} moment of $0.56\mu_B$ while the integrated absolute magnetisation of one supercell is $9.1\mu_B$ (containing 8 Cu^{2+} ions). Given the difficulties in calculating absolute magnetic moments accurately by projecting onto atomic orbitals (such as in a Löwdin analysis), we conclude that the DFT predicts a full Cu^{2+} moment of $1\mu_B$ in the unperturbed system.

If there is any polarised spin density $\rho(\mathbf{r}_\mu)$ at the muon site there is a Fermi contact interaction

$$A = \frac{2\mu_0}{3} \gamma_e \gamma_n \rho(\mathbf{r}_\mu), \quad (1)$$

where γ_μ is the muon gyromagnetic ratio and γ_e is the electron gyromagnetic ratio. The contact hyperfine couplings were calculated using the projector augmented wave (PAW) method⁵ as implemented in the GIPAW package¹ and used norm-conserving data sets with wavefunction cutoff of 120 Ry. These data sets were also used in the calculation of the Löwdin charges used to estimate local magnetic moments.

B. Calculation of the dipolar coupling

The dipolar coupling of the muon with localised magnetic moments \mathbf{m}_i located at position \mathbf{r}_i is given by

$$\mathbf{B}_{\text{dip}}(\mathbf{r}_\mu) = \frac{\mu_0}{4\pi} \sum_i \frac{3(\mathbf{m}_i \cdot \hat{\mathbf{r}}_{i\mu})\hat{\mathbf{r}}_{i\mu} - \mathbf{m}_i}{|\mathbf{r}_\mu - \mathbf{r}_i|^3}, \quad (2)$$

where μ_0 is the vacuum permeability, $\hat{\mathbf{r}}_{i\mu}$ the normalised vector between the muon and the moment \mathbf{m}_i . The dipolar interaction may be evaluated for an infinite sample by calculating the magnetic field given by Eq. 2 within a Lorentz sphere of finite radius r_L . The Lorentz sphere needs to be sufficiently large to reach satisfactory convergence of the calculated field. In our calculations $r_L = 147$ Å. As only antiferromagnetic structures were considered, no further terms need to be considered for the diamagnetic muon sites.

The following magnetic structures were considered (all for the conventional unit cell): (i) Magnetic propagation vector (1/2 0 0) and the two Cu spins parallel or antiparallel, moments along any of the three crystallographic directions. (ii) Magnetic propagation vector (1/2 1/2 0) and the two Cu spins parallel or antiparallel, moments along any of the three crystallographic directions. (iii) Magnetic propagation vector (1/2 1/2 1/2) and the two Cu spins parallel or antiparallel, moments along any of the three crystallographic directions. (iv) Magnetic propagation vector (1/2 0 1/2) and the two Cu spins parallel

or antiparallel, moments along any of the three crystallographic directions. (v) A spiral structure where the two Cu moments are offset by 90° with magnetic propagation vector $(1/2\ 0\ 0)$ with moments in the ab -plane. The latter structure is interesting as it represents the classical solution for a zig-zag spin ladder with frustrating next-nearest-neighbor interactions⁶ as has recently been suggested to occur in $\text{Cu}(\text{pyz})(\text{NO}_3)_2$ on the basis on electron spin resonance measurements⁷. Unfortunately our dipolar field calculations do not allow us to test this hypothesis in $\text{Cu}(\text{pyz})(\text{NO}_3)_2$ as couplings consistent with the experimentally observed values could be reproduced for any of the tested magnetic structures.

The magnetic couplings ν_{dip} were calculated by taking into account the crystallographic distortions within one supercell around the muon (with the muon at the centre) and by taking into account perturbations to the magnetic moments, which were significant for the neutral supercell, by scaling the magnetic moment by the ratio of perturbed and unperturbed Löwdin charge polarization on the Cu ions.

While it is not possible to distinguish between different magnetic structures as, depending on the direction and size of the moment, any one of the structures considered may be consistent with the experimental muon precession frequencies, there is some muon evidence that the moment in $\text{Cu}(\text{pyz})(\text{NO}_3)_2$ must be heavily renormalised from its full value of $1\mu_B$. If the Cu moment were close to $1\mu_B$, we would expect to see oscillations in the range 0.4–16 MHz if we assume all low-energy sites are populated. As the observed oscillations frequencies were $\nu_1(0) = 1.922(4)$ MHz and $\nu_2(0) = 1.257(3)$ MHz and as very slow oscillations $\ll 0.5$ MHz would not be distinguishable from the background due to muons relaxing in the cryostat tail or sample holder, we conclude that a consistent Cu moment size would be around $\mu_{\text{Cu}} \approx 0.12\mu_B$ [$\nu_1(0)/16$ MHz μ_B]. The ordered moment size in low-dimensional magnetic systems is expected to be heavily renormalised by enhanced quantum fluctuations. This value is consistent with the estimate of $\mu_{\text{Cu}} \approx 2.034\sqrt{J_\perp/J} = 0.135\mu_B$ obtained from a mean field model of weakly coupled antiferromagnetic spin chains⁸, where $J = 10.3(1)$ K⁹ is the primary exchange and $J_\perp \approx 0.046$ K is the interchain coupling¹⁰.

We may also predict which (avoided) level crossing resonances are expected in our measurements. There are only two sites where the muon has a sizeable hyperfine contact coupling: one of the nitrate sites (38 MHz, mentioned in the caption) and the carbon sites (≥ 370 MHz). For both oxygen and carbon, the only isotopes with non-zero nuclear spin are not very abundant (O17 has a natural abundance of $< 1\%$ and C13 has an abundance of $\sim 1\%$). Therefore, it is a reasonable assumption that the dominant signal in either case would be a resonance that is a pure muon spin flip (rather than a muon-nuclear flip-flop). These $\Delta M = 1$ resonances for muon and carbon

are at 0.14 T and 1.37 T (for $A = 370$ MHz), respectively. The former is within the range of fields studied. However, level crossing resonances of molecular radicals are typically quite narrow (10s of mT) and hence do not affect the conclusions drawn from the scaling behaviour of λ on much broader scales in field. Furthermore, a muon in most of the possible nitrate sites does not have a contact coupling so the signal from this site (if occupied, it is 200 meV above the ground state) should be small.

	Site	E (meV)	$\nu_{\text{dip}}/\mu_{\text{Cu}}$ (MHz/ μ_B)	A (MHz)
+1	NO ₃	0–200	1.5–12	– ^a
	N(py _z)	140	5.5–16	–
	C(py _z)	1200	–	370
0	NO ₃ (not rot.)	0–170	1.1–9.6	–
	NO ₃ (rot.)	70	1.5–9	–
	N(py _z)	120	0.4–5.6	–
	C(py _z)	420	–	480
	Interst. Mu	2200	–	4640
	Subst. H	–	5.2 – 10.4	< 6

^a In one of the NO₃ sites there is some spin density leakage onto the muon (≈ 38 MHz). Excluding this site does not affect the range of dipolar couplings shown here.

TABLE I. Summary of calculated muon sites and properties for charged (top) and neutral supercells (bottom). Shown are the energy range E , dipolar coupling ν_{dip} for the diamagnetic sites per Cu^{2+} moment of $1\mu_B$, taking all perturbations into account for the interstitial sites and assuming no perturbation for muons substituting on hydrogen sites, and contact hyperfine coupling A .

II. CALCULATED SPIN DENSITY DISTRIBUTION

The calculated spin density is given for four sample sites in Fig. 1. Fig. 1(b) shows the interruption of the magnetic exchange pathway for the nitrate site through the destruction of the Cu moment found for neutral supercells. Fig. 1(c) shows that for the N(py_z) site in the neutral cell, there is a combined effect of (i) switching off the Cu moment and (ii) significantly displacing the Cu ion. Fig. 1(d) shows the same scenario for the charged cell, where only the Cu ion is displaced, leading to an increased magnetic overlap between neighbouring Cu–py_z–Cu chains. While all of these are significant local perturbations that affect the measured dipolar coupling, it is unlikely that any of these would be capable of condensing long-range magnetic order. A summary of all predicted and conceivable muon states and their properties is given in table I.

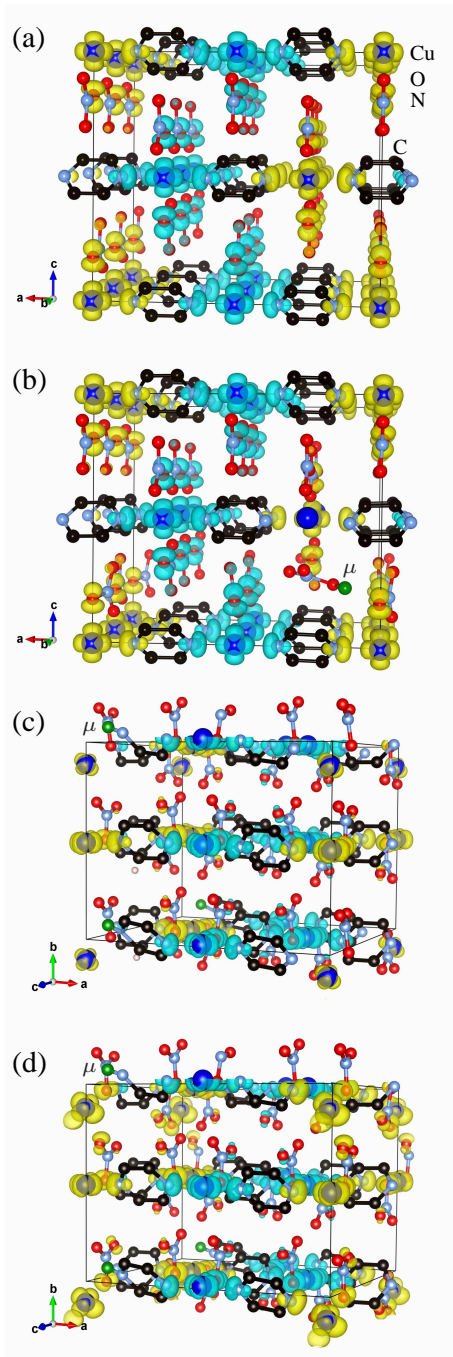


FIG. 1. (color online). Calculated spin density isosurfaces drawn at $0.004/a_0^3$ (a_0 is the Bohr radius). Yellow shading is positive, blue is negative. (a) Unperturbed $\text{Cu}(\text{pyz})(\text{NO}_3)_2$ without a muon showing the quasi-one-dimensional exchange via the pyz rings along the a -axis. (b) For the nitrate site with a rotated nitrate group. This calculation was performed for a neutral supercell. The muon's electron has been donated to the nearest-neighbor Cu ions, turning it into diamagnetic Cu^{1+} . (c) The N(pyz) site for a neutral supercell. The nearest-neighbor Cu ion is displaced considerably and additionally, its moment is destroyed through the donation of the muon's electron. (d) The same nitrogen site but for a charged supercell. The Cu ion is displaced by a similar amount but it retains a magnetic moment, leading to some magnetic overlap between neighbouring Cu–pyz–Cu chains via a nitrate group.

-
- * Present address: Neutron Scattering and Magnetism, Laboratory for Solid State Physics, ETH Zürich, CH-8093 Zürich, Switzerland
- ¹ P. Giannozzi *et al.*, *J. Phys.: Condens. Matter* **21**, 395502 (2009).
- ² J. P. Perdew, K. Burke, and M. Ernzerhof, *Phys. Rev. Lett.* **77**, 3865 (1996).
- ³ D. Vanderbilt, *Phys. Rev. B* **41**, 7892 (1990).
- ⁴ J. Jornet-Somoza, M. Deumal, M. A. Robb, C. P. Landee, M. M. Turnbull, R. Feyerherm, and J. J. Novoa, *Inorganic Chemistry* **49**, 1750 (2010).
- ⁵ P. E. Blöchl, *Phys. Rev. B* **50**, 17953 (1994).
- ⁶ S. R. White and I. Affleck, *Phys. Rev. B* **54**, 9862 (1996).
- ⁷ A. A. Validov, M. Ozerov, J. Wosnitza, S. A. Zvyagin, M. M. Turnbull, C. P. Landee, and T. G. B., *J. Phys.: Condens. Matter* **26**, 026003 (2014).
- ⁸ H. J. Schulz, *Phys. Rev. Lett.* **77**, 2790 (1996).
- ⁹ P. R. Hammar, M. B. Stone, D. H. Reich, C. Broholm, P. J. Gibson, M. M. Turnbull, C. P. Landee, and M. Oshikawa, *Phys. Rev. B* **59**, 1008 (1999).
- ¹⁰ T. Lancaster, S. J. Blundell, M. L. Brooks, P. J. Baker, F. L. Pratt, J. L. Manson, C. P. Landee, and C. Baines, *Phys. Rev. B* **73**, 020410 (2006).